A regressive model for dynamic instabilities during the condensation of R404A and R507 refrigerants

Waldemar Kuczynski*, Tadeusz Bohdal*, Josua P. Meyer, Aleksander Denis***

*Technical University of Koszalin,
Faculty of Mechanical Engineering, Department of Energy
ul. Raclawicka 15-17, 75-620 Koszalin, Poland
Email: waldemar.kuczynski@tu.koszalin.pl
** Department of Mechanical and Aeronautical Engineering
Faculty of Engineering, Built Environment and Information Technology
University of Pretoria
Email: josua.meyer@up.ac.za

Highlights

- Evolution and disappearance of condensation of R507A refrigerant in pipe mini-channels.
- Condensation process occurring in mini-channels.
- Comparison of the results of experimental studies with R404A obtained for R507A.
- Proposition of a regression function for the description of dynamic instability.

Abstract

This paper presents the results of experimental research and mathematical modelling on the influence of dynamic instabilities on the condensation phase change of R507 refrigerant in tubular mini-channels. This agent is currently being utilised as a temporary substitute for R404A, with R448A intended as the target substitute. In addition to the results, this paper contains a dimensional analysis procedure based on the Π-Buckingham theorem that has allowed for the development of a regressive model for the velocities of the dynamic instabilities. The experimental part of this paper was conducted using tubular mini-channels with internal diameters of 1.44, 2.3, and 3.3 mm.

Keywords: Condensation refrigerants, mini-channels, instability, regression function.

1. Introduction

The main motivation for this research was the fact that fluorinated gases, such as hydrofluorocarbons (HFCs), perfluorocarbons (PFCs), sulphur hexafluoride and other agents that contain fluorine, have had to be withdrawn under the Montreal Protocol (1986) and Regulation No. 517/2014 of the European Parliament and of the Council of 16 April 2014. This includes one of the most commonly used refrigerants, R134a. This refrigerant, which includes the R404A refrigerant, has already been withdrawn since 1 January 2017. R1234ze and R1234yf have been suggested as substitutes for R134a, and R507 and R455a have been suggested as substitutes for R404A. The basic parameter that determines the application of these substitutes is their Global Warming Potential (GWP) indicator, which is below 150, as well as the fact that simply withdrawing them reduces fluorinated greenhouse gas emissions by a third (with 2010 as a reference level).

The current state of knowledge has enabled researchers to foresee the influence of hydrodynamic instabilities on the condensation of fluorinated refrigerants in mini-channels. Therefore, an expansion of this knowledge regarding the suggested substitutes is necessary. Research concerning condensation in mini-channels under hydrodynamic instabilities has already been conducted for the refrigerants currently being withdrawn. However, the influence of those instabilities on the phase change of the suggested pro-ecologic substitutes is not known.

It is known that, during the condensation of refrigerants under hydrodynamic instabilities, a propagation of instabilities occurs in a waveform. Two-phase mediums are particularly susceptible to this phenomenon. This propagation of instabilities, which takes the form of an acoustic wave or the wave change of other parameters, such as the density of mass or the heat flux, plays a special role. They all have their own characteristics, with obviously different propagation velocities. Both mechanisms include irreversible dissipation and dispersion. Through their irreversibility, the dissipative effects cause an entropy generation and

dump the instability propagation in a two-phase medium. The dispersive effects influence the instability propagation, which is a function of the generation frequency. The hydrodynamic instabilities in the multi- and two-phase mediums during flow condensation in mini-channels can take different forms. These instabilities result from the characteristics of the instability that induced them, which include the following:

- The beginning of the phase change
- Dynamic change of the mass flux density
- Flow rate
- Pressure
- Temperature
- Void fraction
- Shockwave
- Kelvin-Helmholtz (interference of the surface waves)

The occurrence of the wave phenomena is characterised by a correlation between all of the system's state parameters. For example, a hydrostatic or hydrodynamic change of a mass flux density in the system changes all other parameters, such as the density, pressure, temperature and void fraction. One instability can induce another, and they consequently overlap. An increase in the instability propagation, especially in the waveform, can occur as well. This project aims to identify the qualitative and quantitative description of the phenomena accompanying the condensation of the refrigerants' pro-ecologic substitutes, which are currently being used in mini-channels under hydrodynamic instabilities. The conclusions that result from the theoretical and experimental analysis of these phenomena should affect the development of the current methods' descriptions and supplement the knowledge in this field. It is worth mentioning that there is currently no significant literature in this field.

The research has focused on R1234yf (vehicle air conditioning systems) and R1234ze (heat pumps) refrigerants as substitutes for the commonly used R134a, for which Kuczynski and Denis [1] developed an elaborate mathematical model.

This paper covers the R404A refrigerant, which is dedicated to air conditioners and heat pumps. This refrigerant is currently being replaced by R507. The latter is considered as a transitional substitute, since the final substitute will be either R448A or R452A. All refrigerants have their own physical and thermodynamic properties, and the differences among them can be quite significant. The most important parameters (determining the size and safety of the system) are the latent heat and saturation pressure. Figure 1 shows an example of the saturation pressure versus the temperature curve for the selected refrigerants, as presented by Jung [2]. Most of the refrigerants operate at a similar pressure level, except for the natural refrigerant CO_2.

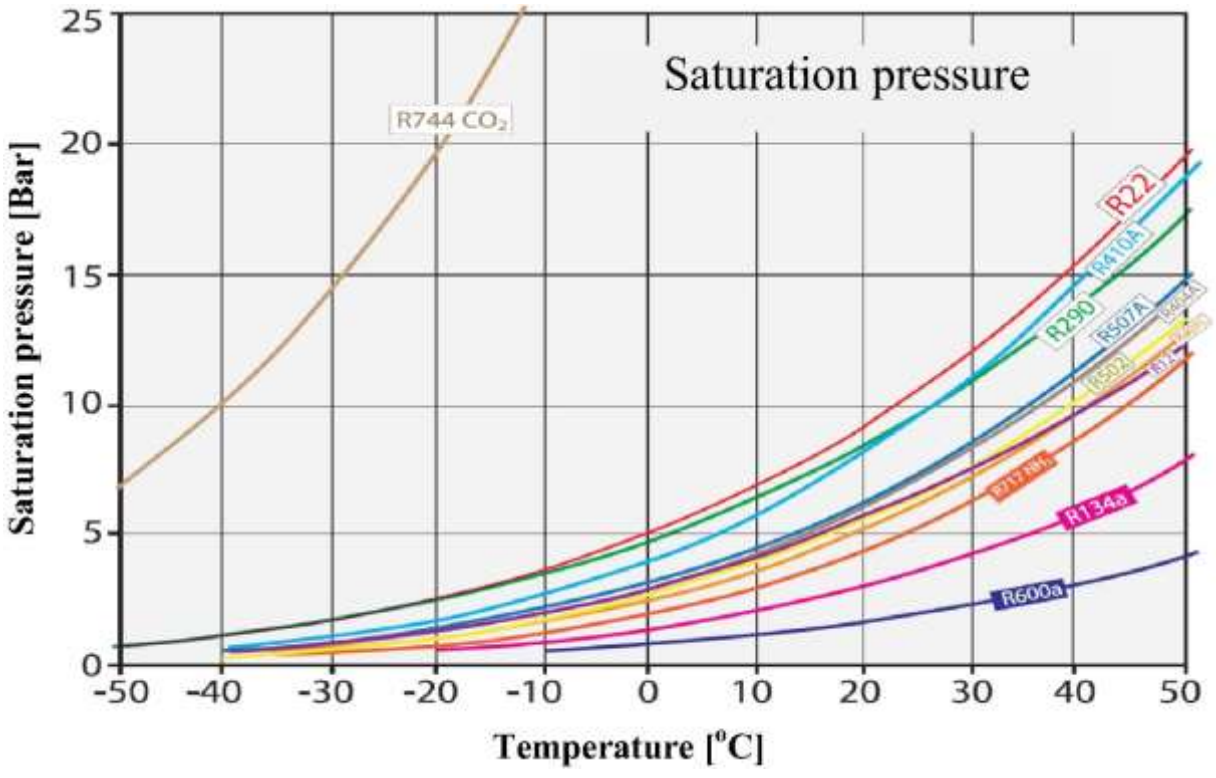

Figure 1: Saturation pressure versus the temperature curve for the selected refrigerants, Jung [2]

Figure 1 shows that the properties of R404A and R507 are quite similar.

2. Thermodynamic properties of the pro-ecological environmentally friendly refrigerant R507

According to the data provided by such producers as Schiessl or Linde, presented by Bonca, Butrymowicz, Targanski and Hajduk [3], the R507 refrigerant is an azeotropic blend with the following composition: 50% penta-fluoro-ethane (R125) and 50% 1,1,1 tri-fluoro-ethane (R143a). At an ambient temperature, it is stored in a liquid state under a high pressure. It has a wide range of applications in low-, medium- and high-temperature refrigeration systems. R507 is currently widely used in industrial refrigeration (cold stores and freezers), commercial refrigeration (supermarkets), air conditioning systems and mobile refrigeration systems. Due to its chemical composition, it requires centrifugal compressors and systems with flooded evaporators. According to current fluorinated gas regulations, R507 is being replaced by low-GWP refrigerants, such as R407F, R448A or R744. However, before the process is completed, R507 will be used as a replacement for R404A.

Table 1 presents the thermodynamic properties of the R404A, R507 and R448A refrigerants included in the Bitner Company Report on Refrigerants [4].

Kuczynski, together with other authors [5–8] such as Teng, Cheng and Zhao [9] and Zhang et al. [10], have presented experimental research on the influence of dynamic instability on the condensation of R404A refrigerant. This paper presents the experimental results for the same conditions, but for another refrigerant, namely, R507. It is vitally important to fully understand the phenomena accompanying the phase changes in tubular mini-channels under unstable conditions.

Table 1. Properties of refrigerants [3].

Type	Pure/blend	ODP	GWP	Safety class	Application	Saturation temperature t'(1bar)	Critical temperature tkr.
HFC - R404A (available until 2020)	Zeotropic blend 143a/125/134a	0	3922	(A1) non-toxic, non-flammable	Large refrigeration systems	-47^{o}C	73^{o}C
HFC - R507	Azeotropic blend R125/R143A	0	3985	(A1) non-toxic, non-flammable	Large refrigeration systems	-47^{o}C	71^{o}C
HFC/HFO - R448A	Zeotropic blend R32 / R125 / R134a /R1234ze / R1234yf	0	1387	(A1) non-toxic, non-flammable	Large refrigeration systems	-45^{o}C	83^{o}C

3. Instabilities during condensation in single mini-channels and multiports

According to the literature, the instabilities that occur during evaporation and condensation phase changes in mini-channels have the same characteristics as conventional channels. Their source can come from both static and dynamic forces. However, as reported by Kuczynski [11, 12] and Bohdal, together with various other authors [13–16], the influence of instabilities on the phase change process performed in mini-channels can be different from that in conventional channels.

In the case of the evaporation phase change in mini- or micro-channels and single- or multiports, the onset of static and hydrodynamic instabilities and their influence on the process are well documented. However, a lack of information concerning the instabilities exists during condensation in such systems. Boiling has been investigated by Boure, together with other authors [17, 18], Cheng, Drew and Lahey [19], Kandlikar and other authors [20–22] and Bergles and other authors [23, 24]. They examined and compared the influence of instabilities occurring in both conventional and mini- and micro-channels. Such instabilities come from the rapid bubble growth investigated by Hsu [25] and Kuo et al. [26], the compressible volume instability, the critical heat flux (CHF) instability and the parallel channel instability documented by Koşar, Kuo and Peles [27] and Stoddard et al. [28].

In the case of rapid bubble growth during evaporation in mini- and micro-channels, a bubble that forms during the oscillatory process reaches a size comparable to the hydraulic diameter of the channel. The flow of refrigerant is temporarily blocked while the bubble grows further along the axis of the channel, which causes the flow to reverse from its original direction. The oscillatory movement of the growing vapour bubble then causes compressible volume instability. This instability manifests itself as a sudden rise in the pressure of the liquid in the vicinity of the growing bubble, as well as an oscillatory change in the medium's density.

In mini- and micro-channels, even a small amount of superheated vapour can cause compressible volume instability that eventually leads to CHF instability. This phenomenon can be observed as a sudden dry-out of the channel's wall due to a rapid temperature increase. In the case of parallel channel instability, its occurrence depends on the ratio between the rise in the pressure and the drop in the mass flow rate. Under metastable transition conditions, the system can easily shift to unstable evaporation due to the sudden growth of the vapour bubble and, as a result, there is a simultaneous occurrence of this instability in individual channels of the multiport. It should also be emphasised that, in the case of conventional channels, the onset of instability due to the formation of a vapour bubble and the transition from the metastable region into the unstable region is relatively rare.

Instabilities during the condensation phase change, in both conventional and mini-channels, are strictly connected to the so-called capillary force. Das and Pattanayak [29, 30], Hewitt and Hall-Taylor [31], Nulboonrueng, Kaewon and Wongwises [32] and Teng et al. [9] investigated and documented this phenomenon. It results from the interactions between the vapour phase and the internal surface of the condensate film. The vapour flows through the core of the channel flow with a different velocity than that of the liquid and causes hydrodynamic forces at the interface. The surface tension at the interface grows and causes the condensate film to wave (see Figure 2).

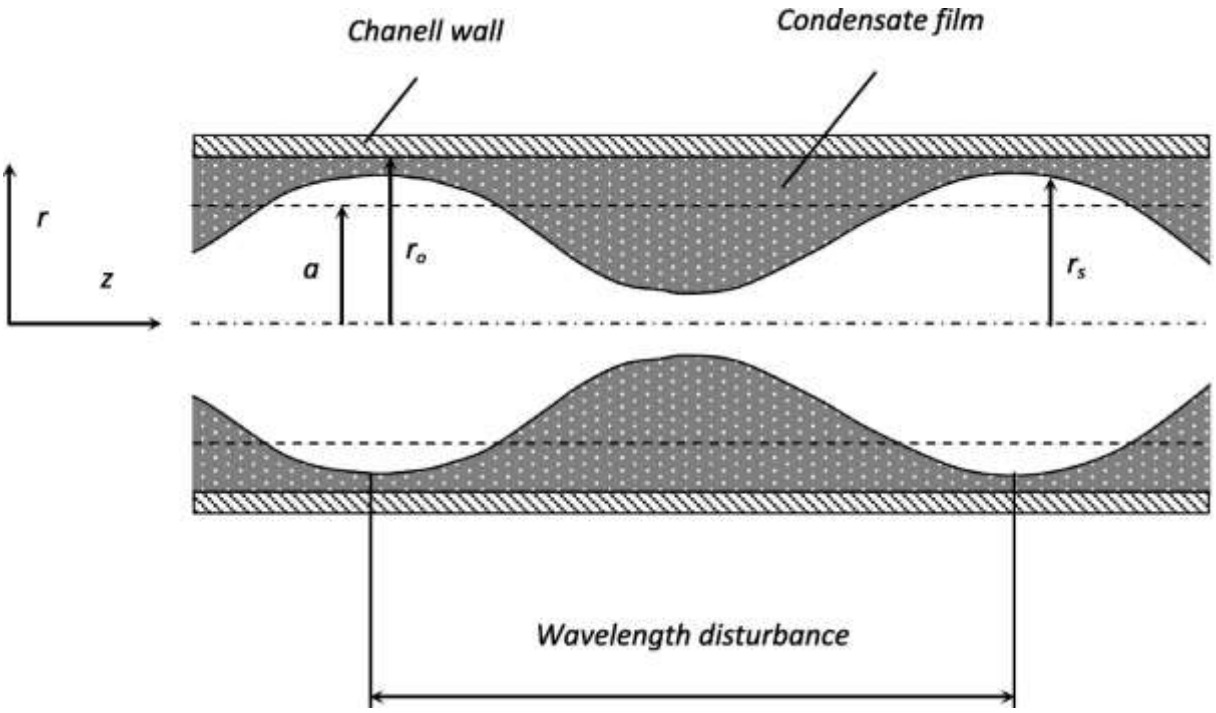

Figure 2: Graphic interpretation of the condensate film waving, Teng et al. [9], Kuczynski [11, 12]

The influence of the capillary forces in conventional channels is not significant, while the disturbance of the liquid phase waving is described by the Kelvin-Helmholtz instabilities [33]. However, in the case of a small channel diameter (such as in mini-channels), the capillary forces play a major role during the phase change process, and the Rayleigh instability model should be used [34].

According to Chen, Groll and Rësler [35], Gauglitz and Radke [36], Ishii and other authors [37–39], the surface of the condensate film is always unstable and waving. As a result, the thickness of the condensate film can reach up to half of the hydraulic diameter of the channel, and so-called liquid bridges will be formed. In the case of a conventional channel, this situation corresponds to the single-phase subcooled liquid zone.

The formation of liquid bridges in mini-channels is a source of instabilities that has been documented by Carey [40], Mercredy, Wigdortz and Hamilton. [41], Middleman [42], Vasilýev, Konev and Razek [43] and Kuczynski [11, 12] as capillary-collar flow, capillary-

bubble flow (see Figure 3) and capillary blocking (see Figure 4). These phenomena are strictly connected to the velocity of the vapour phase in the core of the channel.

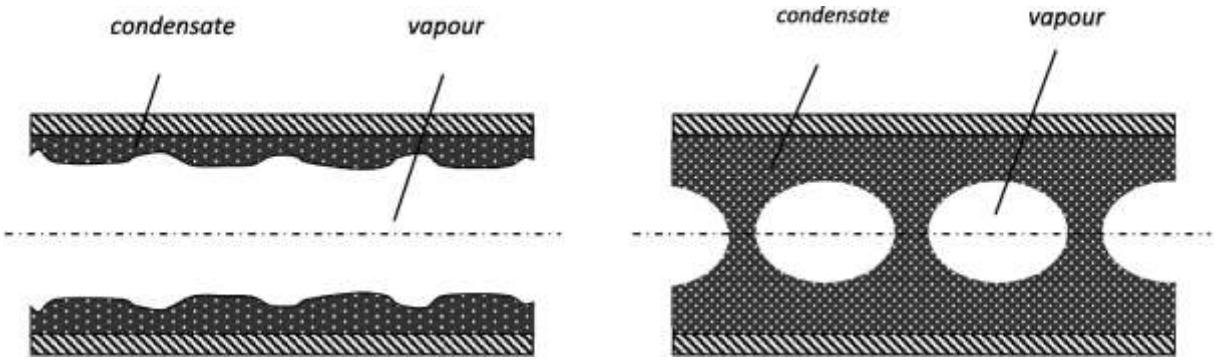

Figure 3: Graphic interpretation of a) the capillary-collar flow and b) the capillary-bubble flow, Teng et al. [9], Kuczynski [11, 12]

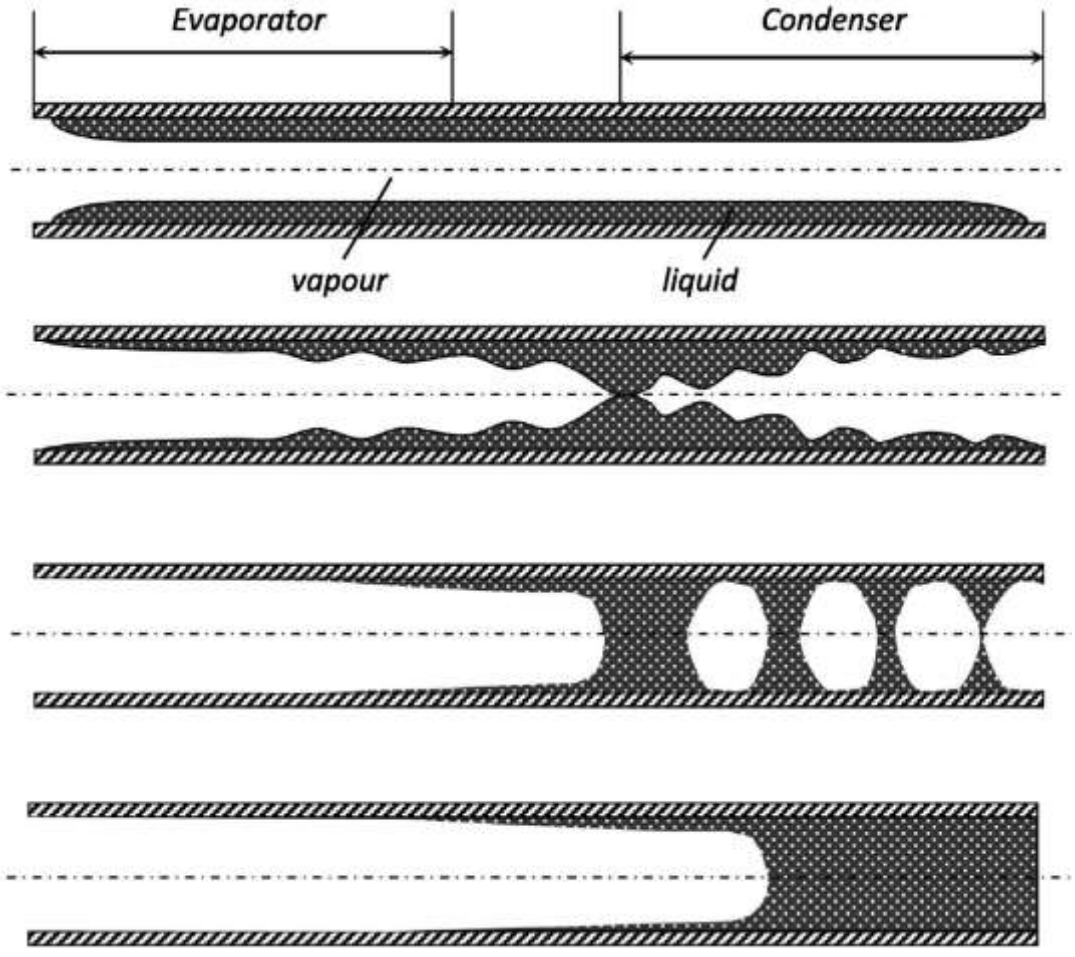

Figure 4: Graphic interpretation of capillary blocking, Tang et al. [9], Kuczynski [11, 12]

According to Sikora [44], Laskowski and Jaworski [45], as well as Grabowski and Blachnio [46], capillary-collar flow occurs when the condensate film is thin, and the high-velocity vapour in the channel core causes the oscillatory waving of the liquid surface. However, according to Henry, Grolmes and Fauske [47], the periodicity of the vapour phase flow causes a constant disturbance wavelength on the condensate surface.

Research conducted by Levy [48], Wallis [49] and Wang, Cheng and Bergles [50] showed that the growth of the condensation film due to a vapour quality drop, which causes a decrease in the vapour velocity, leading to the formation of so-called liquid bridges inside the mini-channels. This results from a direct contact between the points with the highest waving amplitude (half of the channel's hydraulic diameter). The liquid bridges split the vapour phase into separate bubbles, leading to capillary bubble flow. In conventional channels, the liquid bridges grow both upstream and downstream. In the upstream region, the condensate film decays, while in the downstream region, the bubbles collapse due to the condensation process.

In cases where the condensate driving force is not sufficient to overcome the hydraulic resistance, the flow is temporarily blocked. Middleman [42], Mercredy, Wigdortz and Hamilton [51] and Middleman [52] documented this phenomenon as so-called capillary blocking. It occurs in tubular mini-channels with various cross-sectional area shapes. This results from there being a much lower condensate velocity in the mini-channels than in the conventional channels.

In contrast to that of conventional channels, the vapour phase velocity is much lower. Therefore, condensate decay due to the hydrodynamic forces in the upstream region does not occur. Bohdal [13], Martin and Padmanabhan [53] and Starov et al. [54] have investigated this subject. Thus, the liquid bridges in mini-channels always result in capillary blocking and a so-called "dead" region at the end of the condenser, especially in the case of multiports. This is due to the sudden condensation of the vapour bubbles downstream, which leads to the so-called liquid cork. In the case of instabilities during the evaporation phase change in mini-channels,

the sudden expansion of a vapour bubble to the size of the hydraulic diameter of the channel causes a temporary reversal of the flow direction. Such an occurrence of capillary blocking during the condensation process leads to a temporary flow decay. This phenomenon significantly influences the thermal performance of the condensation process inside the mini-channels due to the shrinkage of the high-efficiency two-phase heat exchange zone, which only occurs in channels with an internal diameter below 5 mm. This is strictly connected to the velocity of the gaseous phase.

4. Methodology of the experimental research

4.1. Apparatus

Kuczynski [6] and Kuczynski and Charun [55] have already presented the experimental research's methodology and data processing. The experimental part of this research was conducted using the apparatus shown in Figure 4. The circulation of the refrigerant begins in a tank. The liquid medium leaves the tank at a high pressure and ambient temperature. Next, the pressure of the refrigerant decreases at the expansion valve situated at the inlet to the evaporator, where it absorbs the ambient heat in order to evaporate. Another step takes place in the compressor. This piece of machinery increases the pressure and temperature of the gaseous refrigerant. After leaving the compressor, the refrigerant splits into two streams. The more significant part of the flux returns via the condenser, which turns it back into a liquid, while the smaller part (which can be set with the regulation valve) goes to the test section. The test section has a cut-off valve situated at the inlet, where it introduces the instabilities. The controller regulates the valve's timings.

The test section, as shown in Fig. 5, consists of a mini-channel equipped with pressure sensors and type-K thermocouples. This mini-channel is immersed in a water bed that removes heat. An additional water pre-conditioner cools the water at a constant temperature. The

aftercooler condenses the remaining gaseous refrigerant that has exited the test section, while the refrigerant passes in a liquid state through a flow meter and goes back to the mainstream to close the inner loop. As the signals from pressure, temperature and flow sensors are analogue, they need to be converted into digital signals. To do this, A/D adapters are used with the digital signals and are eventually processed and stored on a computer (Fig. 6)..

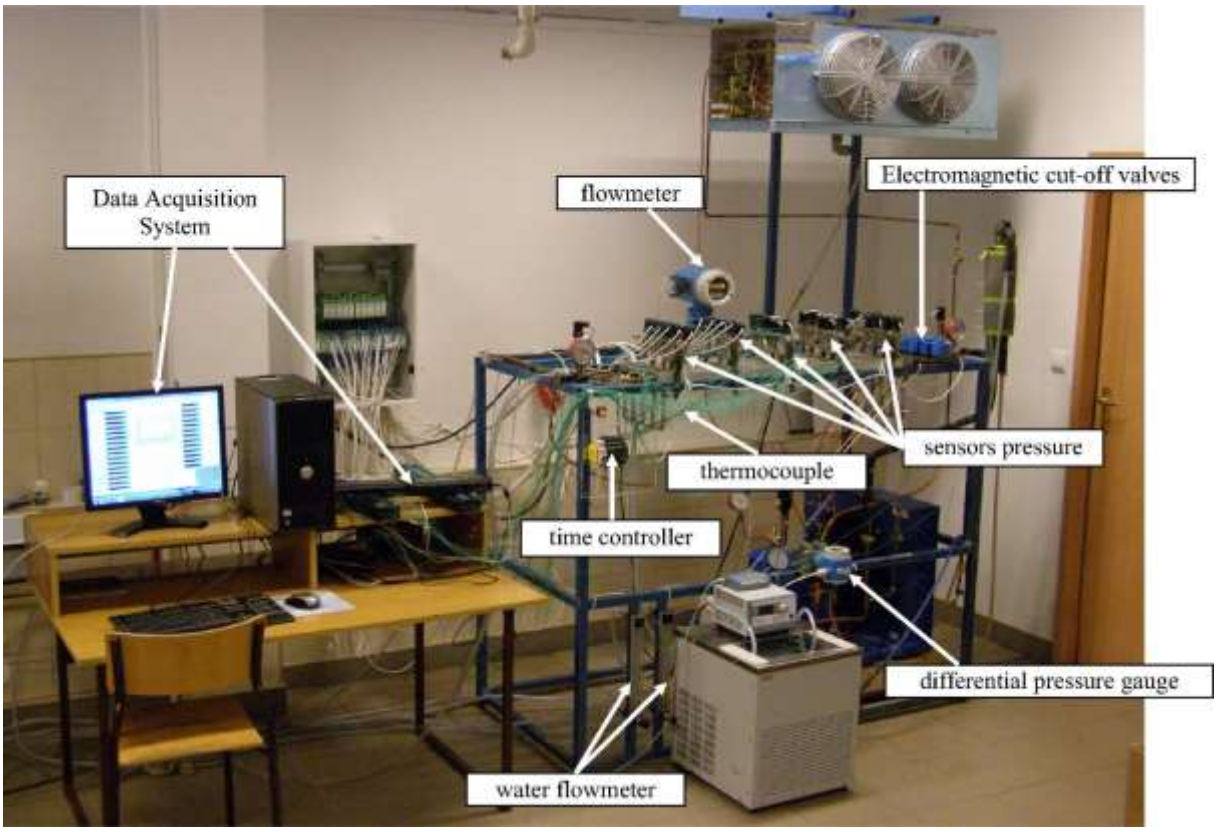

Figure 5: View and scheme of the apparatus

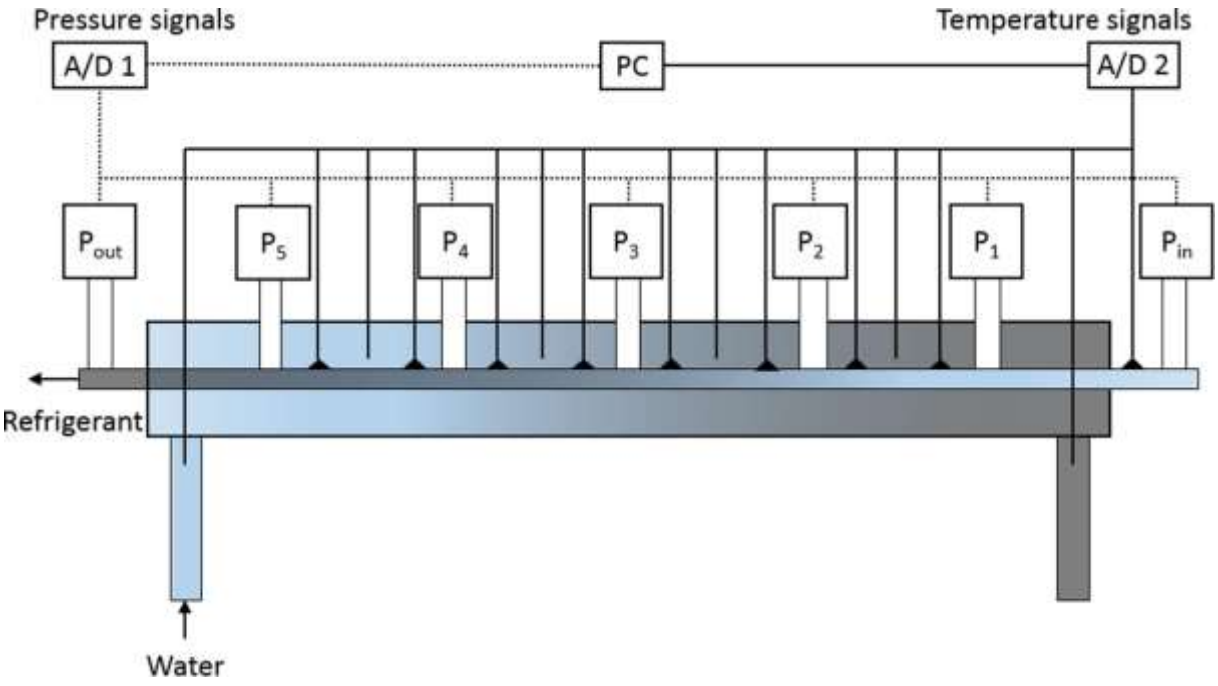

Figure 6: Scheme of the test section

The experimental conditions for the R404A and R507 refrigerants were as follows:

- Three internal diameters (IDs) = {3.3; 2.3; 1.44 mm}
- Single channel configuration
- Refrigerant mass flux of G = 60 ÷ 316 kg/(m^2·s)
- Refrigerant inlet pressure of p_{in} = 1.09 ÷ 1.17 MPa (saturation temperature t_{sat} = 42.6 ÷ 45.5 [^{o}C)])

A series of experiments conducted within the abovementioned parameter limits allows one to obtain detailed data concerning the evolution of the mass flow rate, the pressure distribution and the temperature distribution over time along the test section under both steady-state and periodic disturbance conditions. Samples of the acquired data are shown in Figures 7, 8 and 9. The characteristics of the curves are very similar to those obtained by Kuczynski and Charun [5] for the R404A refrigerant.

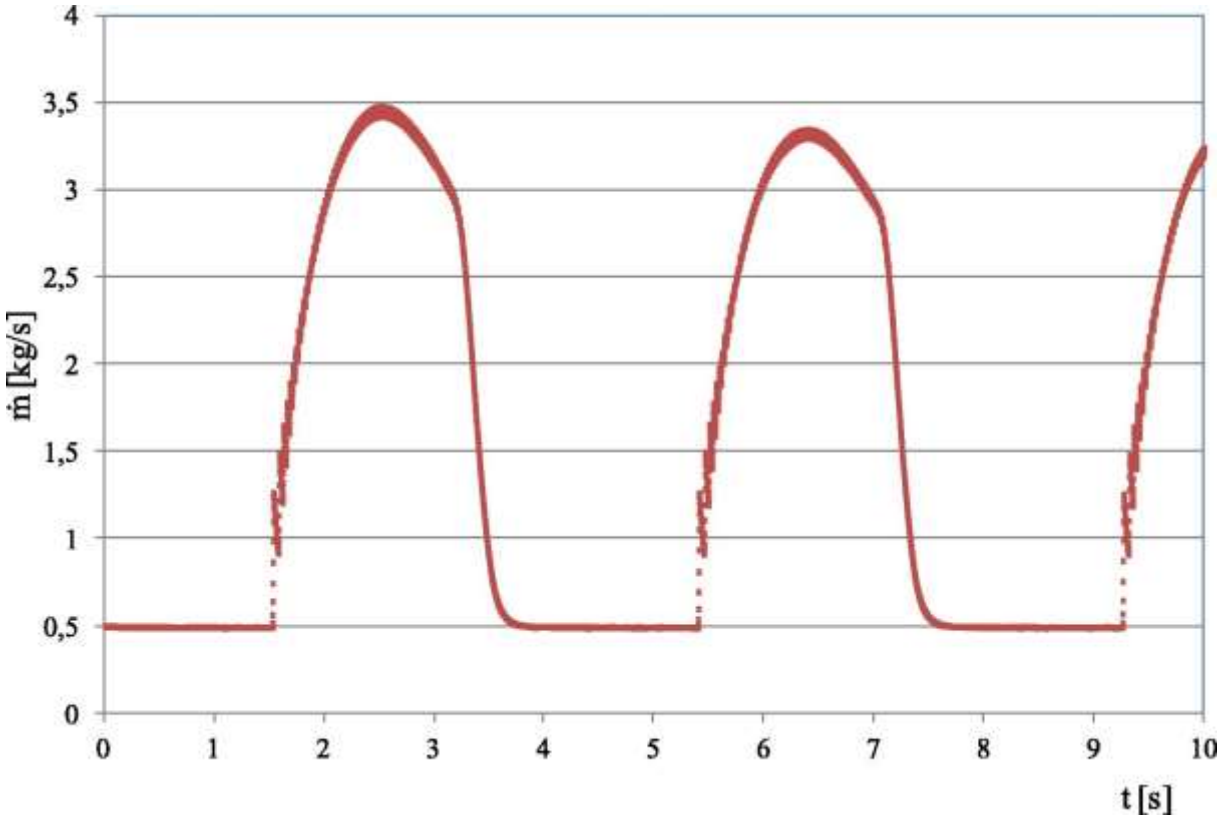

Figure 7: Sample of flow oscillations for ID = 2.3 mm

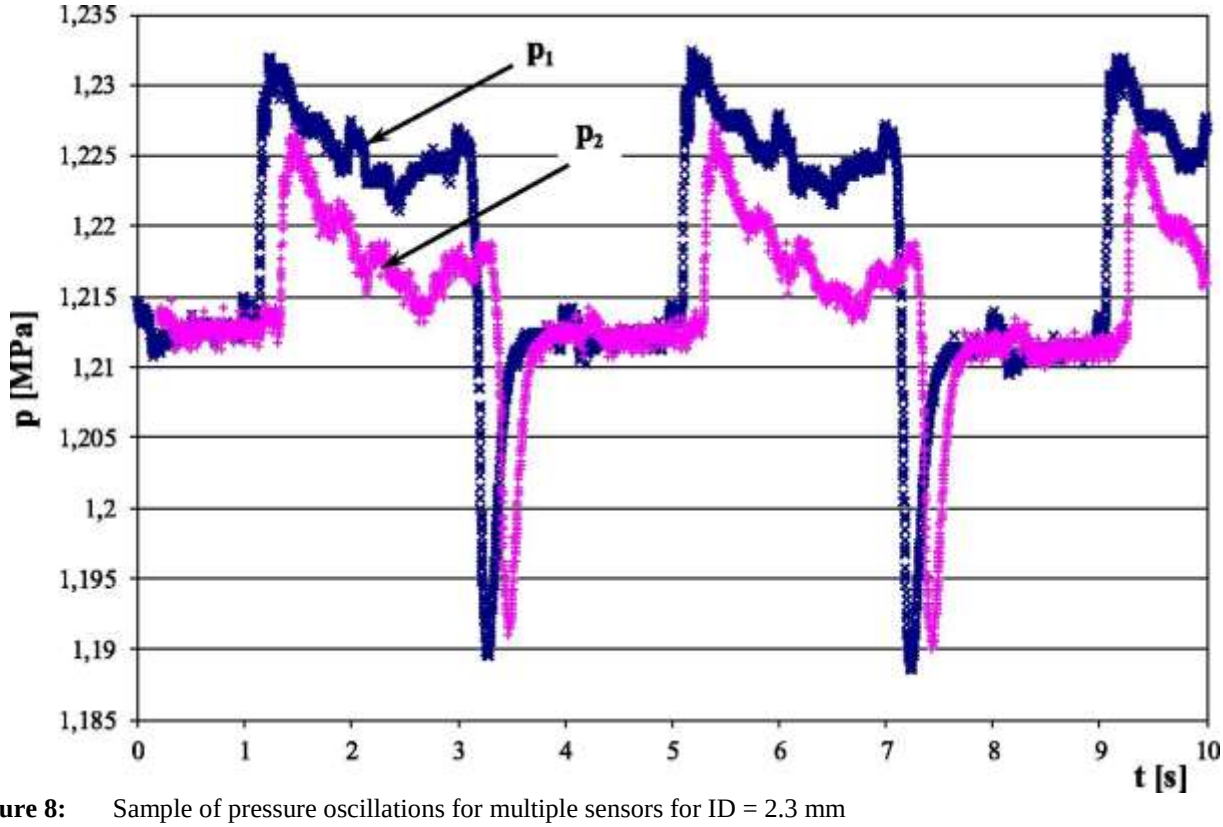

Figure 8: Sample of pressure oscillations for multiple sensors for ID = 2.3 mm

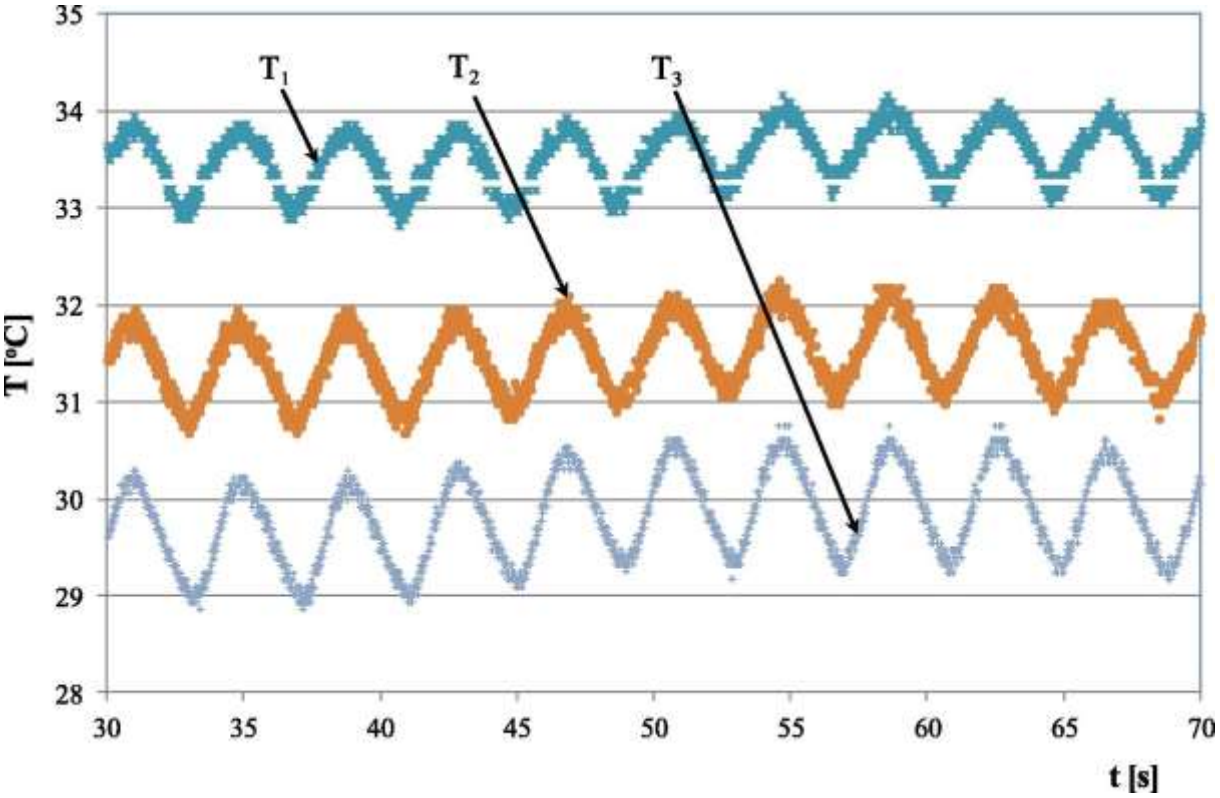

Figure 9: Sample of temperature oscillations for multiple sensors for ID = 3.3 mm

The experimental results allow one to determine the velocities of the instabilities. Figure 9 shows the velocities of the pressure instabilities v_p as a function of frequency for different IDs and two refrigerants, R507 and R404A, obtained by Kuczynski and Charun [5]. Figure 10 shows the velocities of the temperature instabilities v_T.

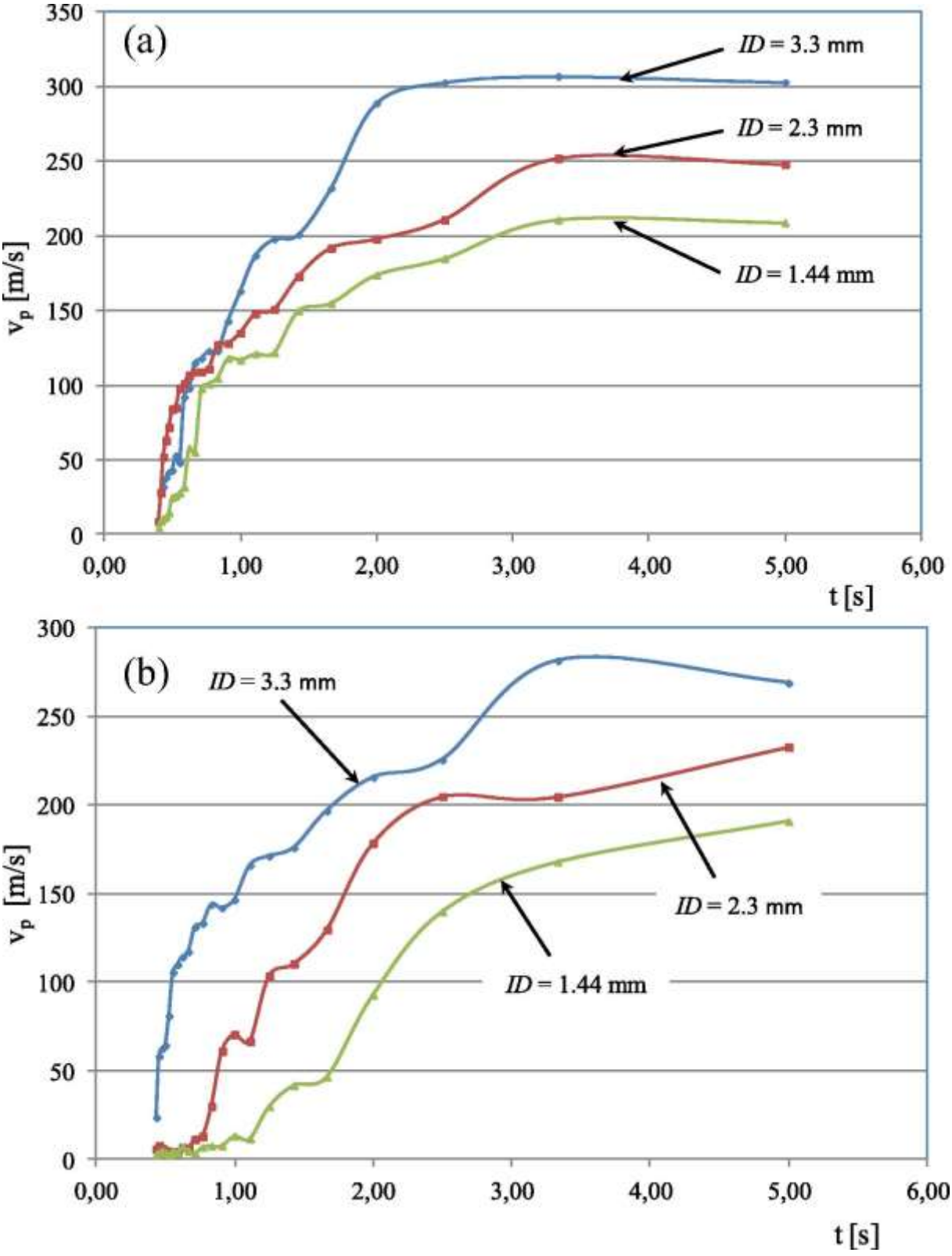

Figure 10: Velocity of the pressure instabilities v_p as a function of frequency f for different IDs: a): R507 refrigerant; b): R404A refrigerant

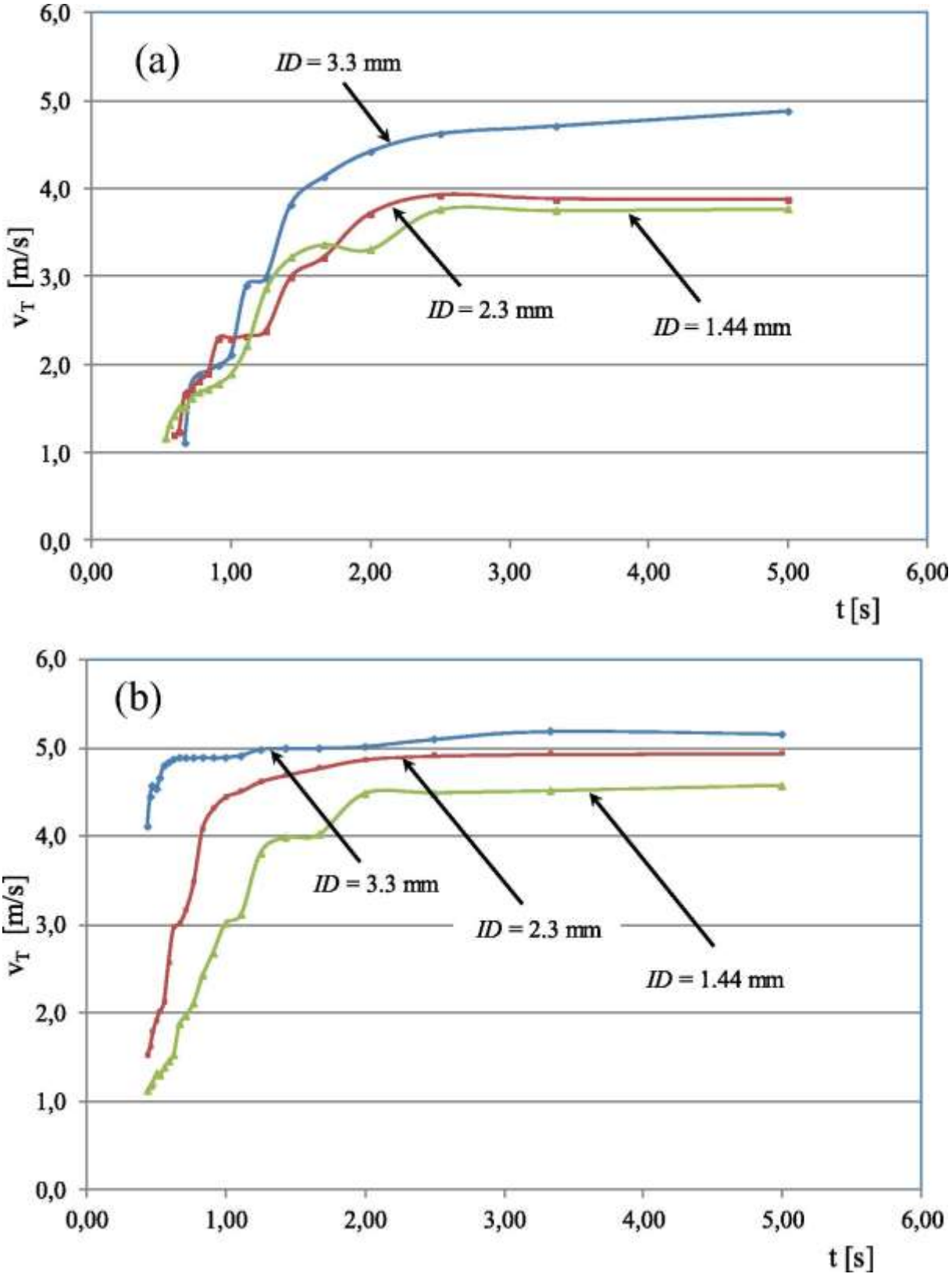

Figure 11: Velocity of the temperature instabilities v_T as a function of frequency f for different IDs: a): R507 refrigerant; b): R404A refrigerant

Based on the experimental velocities of the pressure v_p (see Figure 10) and temperature v_T (see Figure 11) instabilities, a mathematical formula was obtained using the regression scheme. The next section of this paper presents the development process of the mathematical models for different instabilities and refrigerants.

5. Evaluation of measurement errors

In this example, the changes in the signal's movement velocity (oscillation) for pressure v_P and for temperature (condensation front) v_T in the condenser (pipe mini-channel) are experimentally determined, and the procedure for determining the measurement uncertainty is presented. . The values of v_{Pi} and v_{Ti} were characterised by a noticeable "scattering" from the mean values of $\bar{v}_P$ and $\bar{v}_T$, i.e., standard deviation.

Determining the movement velocity of the pressure and temperature change signal was connected with determining (in dynamic conditions of generated disturbances) time *t*, in which the pressure and temperature changes of the signal move along the length of the pipe mini-canal. On the basis of point estimation, the results of the measurements were determined:

- average value estimator:

$$\bar{x} = \frac{1}{n}\sum_{i=1}^{n} x_i \tag{1}$$

- standard deviation estimator:

$$\bar{S}_{\bar{x}} = \sqrt{\frac{1}{(n-1)}\sum_{i=1}^{n}(x_i - \bar{x})^2} \tag{2}$$

which is expressed as y_A - type *A* uncertainty of measurement.

For the

confidence interval $\alpha = 0.9$, it was assumed that the accuracy q_α is defined as the absolute mean deviation for the number of measurements n = 19 and the values Δt_p and Δt_T will not exceed q_α = 0.4 of the standard deviation estimator value $\bar{S}_{\bar{x}}$. The value of q_α is defined as follows:

$$q_\alpha \overset{def}{=} \frac{t_\alpha}{\sqrt{n}} \tag{3}$$

where:

$$t_\alpha = \frac{\bar{x} - x_i}{\bar{S}_{\bar{x}}}\sqrt{n} \tag{4}$$

They use tables [58] to specify that for $\alpha = 1 - 0.9$ and $q_\alpha = 0.4$, the number of measurement-rates may not be less than $n = 19$. Following this rule, it was determined that the number of experiments will be $19 < n < 120$ for each of the tested mini-channels.

To estimate the uncertainty of the measuring apparatus, the measured values of the measurands were used, treating them as an estimator of the expected value expressed as a formula:

- uncertainty of type u_B:

$$u_B = \frac{\Delta_g}{\sqrt{3}} \tag{5}$$

where Δg is the limit of the error, which is determined on the basis of the instrument's accuracy class, which usually calculated from an expression:

$$\Delta_g = \frac{Z \cdot K}{100} \tag{6}$$

The standard uncertainties of types *A* and B are used for assessing the overall uncertainty of the measurement in the intermediate measurements. The overall standard uncertainty of the measurement was determined:

$$u_Ł = \sqrt{u_A^2 + u_B^2} \tag{7}$$

where the standard uncertainty for the mean value takes the form:

$$u_{\bar{y}} = \sqrt{\sum_{j=1}^{n}\left(\frac{\partial y}{\partial x_i}\cdot u_L\right)} \tag{8}$$

It follows that the absolute error y (standard uncertainty) of the quantities indirectly determined $y = f(x_1, x_2, x_3, ...x_n)$, which will be calculated according to the formula:

$$\Delta y = \sqrt{\left(\frac{\partial f}{\partial x_1}\Delta x_1\right)^2 + \left(\frac{\partial f}{\partial x_2}\Delta x_2\right)^2 + \left(\frac{\partial f}{\partial x_3}\Delta x_3\right)^2 + ... + \left(\frac{\partial f}{\partial x_n}\Delta x_n\right)} \tag{14}$$

where $\Delta x = u_B$, while the relative error is determined from the dependency:

$$\delta y = \frac{\Delta y}{y}\cdot 100\% \tag{15}$$

In the case of using a measuring card with a sampling frequency of 10^{-6} Hz (for time shift measurement), it is possible to perform measurements at a rate of 10^6/s. However, taking the limitations resulting from the technical capabilities of the computer used in the tests into account, a maximum of 10^3 measurements per second were assumed, which was considered as a slowdown.

The calculation of the total standard uncertainty of measurement is shown in the example. For the pressure measurement, *Endress Hauser* piezoelectric sensors, with an accuracy class k = 0.5% and a range $Z = 0 \div 1.6$ MPa, were used. The standard uncertainty of the measurements of uA was assumed to be at a level 0.8 kPa:

$$\Delta p = \sqrt{800^2 + \left(\frac{1600}{\sqrt{3}}\right)^2} = 1222{,}02 Pa \tag{16}$$

Similarly, other values were determined, which are presented in Table 1.

Table 2. Summary of measurement errors.

Values determined experimentally	**Standard uncertainty of measurement**
Pressure p	$\Delta p = \sqrt{800^2 + \left(\frac{1600}{\sqrt{3}}\right)^2} = 1222{,}02Pa$
Mass flow $\dot{m}$	$\Delta\dot{m} = \sqrt{0{,}005^2 + \left(\frac{100}{\sqrt{3}}\right)^2}\left[\frac{kg}{h}\right]$
Temperature T	$\Delta T = \sqrt{0{,}05^2 \cdot \left(\frac{0{,}05}{\sqrt{3}}\right)^2} = 0{,}06K$
Channel cross-sectional area A	$\Delta A = 0{,}0000001\ [m^2]$
Distance between sensors	$\Delta l = 0{,}001\ [m]$
Indirectly determined figures	***Calculated maximum error***
Pressure differences Δp	$\Delta p = \pm 0{,}0008MPa$
Movement speed signals change of pressure v_p and temperature v_T,	$\delta\Delta v = \pm 6\%$
density of the mass flux (G)	$\Delta(G) = \pm 0{,}0022 \div 0{,}00042\frac{kg}{m^2 s}$

6. Regression model for the R404A and R507 refrigerants

Using the regression scheme that was presented in Kuczyński [11,12] of this paper and the dimensional analysis, the following formula for the dimensionless velocity of the pressure instabilities was derived:

$$v_p^+ = C \cdot \mathrm{Re}_{TPF}^{a_1} \cdot \Delta p^{+a_2} \cdot \Phi^{a_3} \tag{17}$$

and for the temperature instabilities:

$$v_T^+ = c \cdot \mathrm{Re}_{TPF}^{a_1} \cdot \Delta T^{+a_2} \cdot \Phi^{a_3} \tag{18}$$

Equations 1 and 2 were linearised with the following double-sided logarithm:

$$\log v_p^+ = \log C + a_1 \cdot \log \mathrm{Re}_{TPF} + a_2 \cdot \log \Delta p^+ \cdot \log \Phi\,, \tag{19}$$

A regression scheme was used to calculate the constant C and the exponents: a_1, a_2 from equations 1 and 2. These calculations used Statistica software. The compensation calculations were made for 196 equations, which represent the experimental results on the concerned instabilities.

In the case of pressure instabilities, the following constants were obtained for Equation 1:

C = 46379; a_1 = -2.27; a_2 = -3.81; a_3 = 2.13 with a variance of 98% and a correlation coefficient of R = 0.98.

Thus, Equation 1 obtains its final form as:

$$v_p^+ = 46379 \cdot \mathrm{Re}^{-2.27} \cdot \Delta p^{+\,-3.81} \cdot \Phi^{-2.13}. \tag{20}$$

The empirical Equation 20 was validated within the limits given in Section 3 of this paper. The model's agreement with the experimental values is quite good, with most of the points falling in the range of ± 25%, as shown in Figure 12.

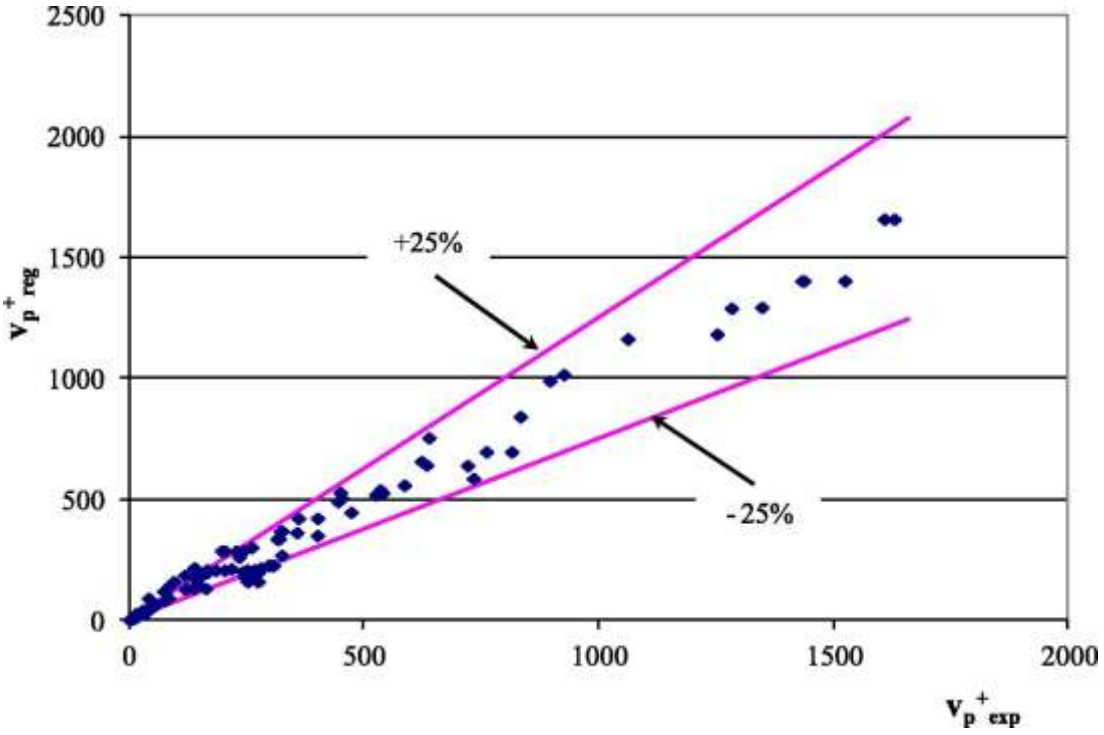

Figure 12: Relationship between the dimensionless velocity calculated according to the derived formula $v_p{}^+{}_{reg}$ and the experimental results $v_p{}^+{}_{exp}$

The same procedure was performed for the temperature instability, and the following constants were obtained: C = 0.11; a_1 = -0.34, a_2 = -2.04; and a_3 = 0.49, with a variance of 94% and a correlation coefficient R = 0.90.

Thus, Equation 3 obtained its final form as:

$$v_T^+ = 0.11 \cdot \mathrm{Re}_{TPF}^{-0.34} \cdot \Delta T^{+-2.04} \cdot \Phi^{0.49} \quad (21)$$

The empirical Equation 21 was validated within the limits provided in Section 3 of this paper. The agreement of the model with the experimental values is quite good, with most of the points falling in the range of ± 25%, as shown in Figure 13.

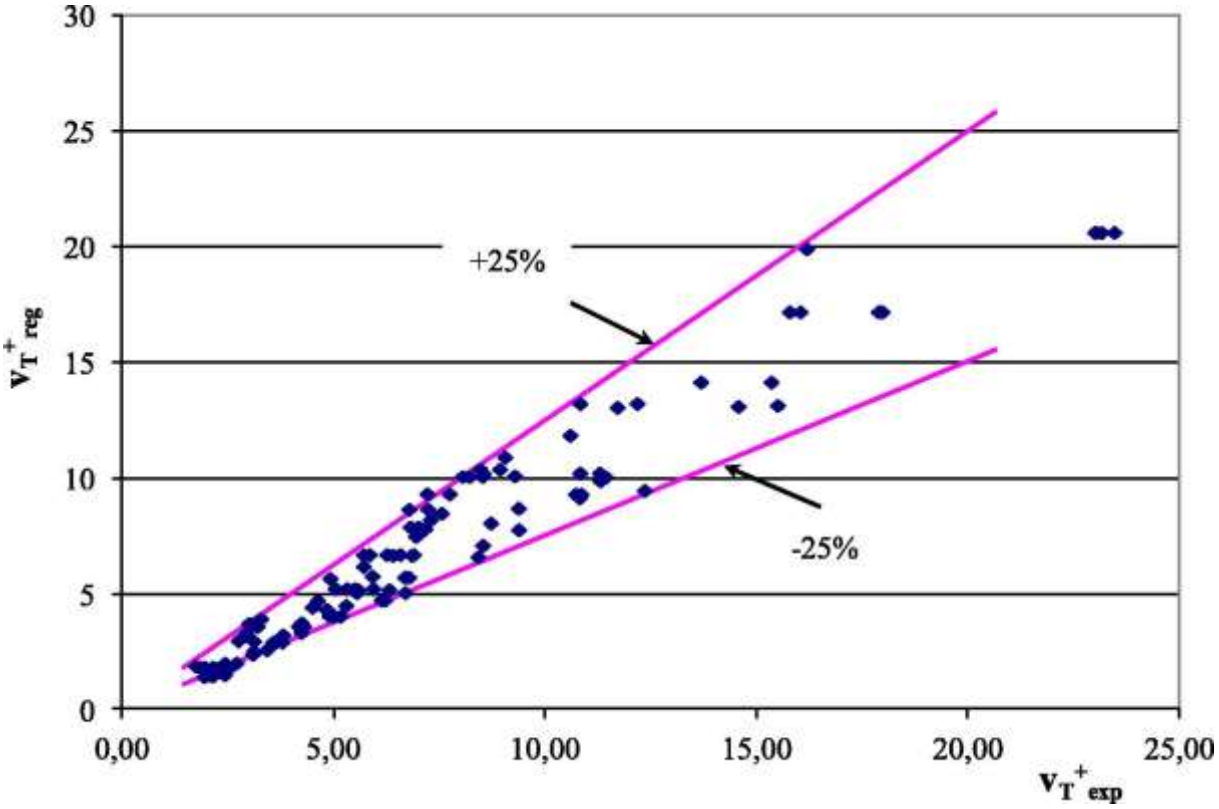

Figure 13: Relationship between the dimensionless velocity calculated according to the derived formula $v_T^+{}_{reg}$ and the experimental results $v_T^+{}_{exp}$

It was determined that the velocities of the pressure v_p and temperature v_T instabilities are interdependent. Their dimensionless equivalents v_T^+ and v_p^+ are also interdependent, as shown in Figure 14.

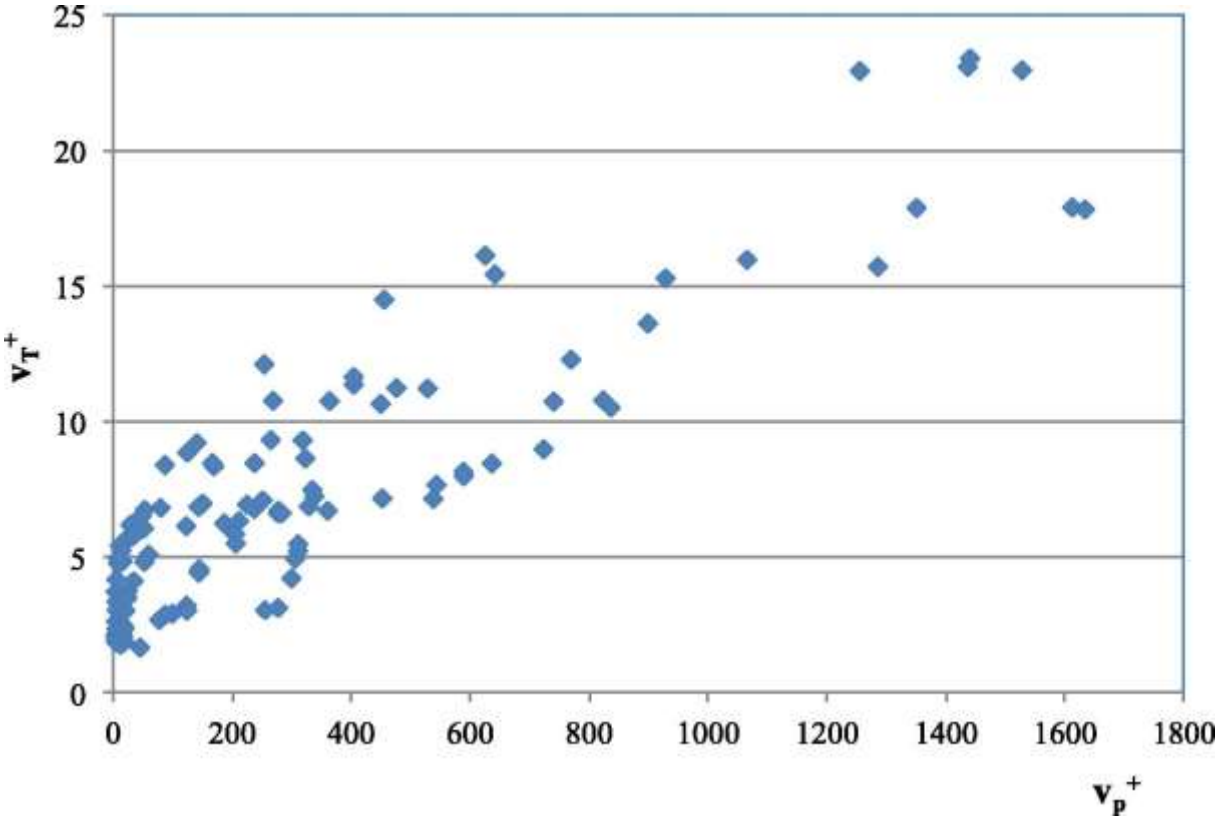

Figure 14: Interdependency between the dimensionless velocity of the temperature instability v_T^+ and dimensionless velocity of the pressure instability v_p^+

The relationship shown in Figure 14 means that, for the condensing two-phase medium, the value of the pressure is strictly connected to the value of the temperature. Therefore, Equation 21 for the dimensionless velocity of the temperature instability v_T^+ can be rewritten, while the dimensionless temperature drop ΔT^+ can be substituted by the dimensionless pressure drop Δp^+. The constants of the new Equation 21 are as follows:

$C = 0.01$; $a_1 = 0.92$; $a_2 = -2.87$; $a_3 = 2.52$; with a variance of 88% and a correlation coefficient of $R = 0.94$.

$$v_T^+ = 0.01 \cdot \mathrm{Re}_{TPF}^{0.92} \cdot \Delta p^{+\,-2.87} \cdot \Phi^{2.52}, \tag{22}$$

Equations 20 and 21 are equivalent, and they can be used alternatively, depending on the assumptions and the actual needs.

7. Conclusions

The second part of this article covered the experimental results concerning the influence of dynamic instabilities on the condensation of the R507 refrigerant in tubular mini-channels. The R507 refrigerant is a temporary, pro-ecological and environmentally friendly substitute for R404A, and R448A is the final substitute. The experimental research was conducted in the same manner as for the R404A refrigerant with the following results:

- The velocity of the pressure instabilities v_p ranged between 5 and 303 (m/s), which matches the range previously obtained for R404A, 2–269 (m/s).
- Based on the experimental results, a mathematical model for the dimensionless velocity of the pressure instabilities v_p^+ was derived. The agreement between the model and the experimental results was quite good, with most of the points falling in a range of ± 25% with a variance of 94% and a correlation factor coefficient of R = 0.97.
- The velocity of the temperature instability v_T ranged between 1 and 4.9 (m/s), which matches the range previously obtained for R404A, 1–5.2 (m/s).
- Based on the experimental results, a mathematical model for the dimensionless velocity of the temperature instabilities v_T^+ was derived. The agreement between the model and the experimental results was quite good, with most of the points falling in a range of ± 25% with a variance of 95% and a correlation factor coefficient of R = 0.98.
- This paper included an alternative model for the dimensionless velocity of the temperature instabilities v_T^+, which was based on the dimensionless pressure drop Δp^+ instead of the dimensionless temperature drop ΔT^+. In this case, the agreement between the model and the experimental results was quite good, with most of the points falling

in a range of ± 25%, although the variance was only 88% and the correlation factor coefficient only $R = 0.94$.

Therefore, it may be assumed that the presented models are sufficient for qualitatively and quantitatively describing the velocities of dynamic instabilities in mini-channels.

The enclosed appendix covers the methodology of the dimensional analysis and the regression scheme used in this article. This entire process was based on the process developed by Kukielka [56] and Roeske-Slomka [57].

Appendix

To derive formulas for the velocities of the pressure v_p and temperature instabilities v_T, a dimensional analysis, together with the Π-Buckingham theorem, was used. The main assumption of this method is that the number of dimensionless modules equals the number of variables reduced by the number of independent dimensions, such as metre, second, kilogram and Kelvin.

The velocity of the pressure instability v_p depends on the following parameters:

$$v_p = f(\Delta p, p_o, \nu', d, w, \Phi) \tag{A.1}$$

Table A.1 contains the dimensional analysis of the parameters that influence the velocity of the pressure instability v_p.

Table A1. Dimensional analysis of parameters that influence the velocity of the pressure instability v_p.

Parameter	SI units			Role
	[kg]	[m]	[s]	
v_p	0	1	-1	Target function
Δp	1	-1	-2	Term of Π_1 eq.
p_0	1	-1	-2	Independent parameter
v'	0	2	-1	Independent parameter
d	0	1	0	Independent parameter
w	0	1	-1	Term of Π_2 eq.
Φ	0	0	0	Dimensionless

The first step is to verify that the selected independent parameters are independent of one another. To do so, the determinant for the p_0, v', d dimensions has to be a number other than zero:

$$\det\begin{bmatrix} 1 & -1 & -2 \\ 0 & 2 & -1 \\ 0 & 1 & 0 \end{bmatrix} = 1 \tag{A.2}$$

The next step is to derive dimensionless numbers Π_1 and Π_2.

Π_1 base equation:

$$\Delta p = \Pi_1 p_o^{a_{11}} v'^{a_{12}} d^{a_{13}} \tag{A.3}$$

and the corresponding set of dimensional equations:

$$\left[kg^1 m^{-1} s^{-2}\right] = \left[kg^1 m^{-1} s^{-2}\right]^{a_{11}} \cdot \left[kg^0 m^2 s^{-1}\right]^{a_{12}} \cdot \left[kg^0 m^1 s^0\right]^{a_{13}}, \tag{A.4}$$

$$kg: 1 = 1 \cdot a_{11} + 0 \cdot a_{12} + 0 \cdot a_{13}, \tag{A.5}$$

$$m: -1 = -1 \cdot a_{11} + 2 \cdot a_{12} + 1 \cdot a_{13}, \tag{A.6}$$

$$s: -2 = -2 \cdot a_{11} - 1 \cdot a_{12} + 0 \cdot a_{13}, \tag{A.7}$$

which gives:

$a_{11} = 1$, $a_{12} = 0$, $a_{13} = 0$,

so the Π_1 equation obtains its final form as:

$$\Delta p = \Pi_1 p_o^1 v'^0 d^0 \Rightarrow \Pi_1 = \frac{\Delta p}{p_0}, \tag{A.8}$$

Π_2 equation:

$$w = \Pi_1 p_o^{a_{21}} v'^{a_{22}} d^{a_{23}}, \tag{A.9}$$

and the corresponding set of dimensional equations:

$$\left[kg^0 m^1 s^{-1}\right] = \left[kg^1 m^{-1} s^{-2}\right]^{a_{21}} \cdot \left[kg^0 m^2 s^{-1}\right]^{a_{22}} \cdot \left[kg^0 m^1 s^0\right]^{a_{23}} \tag{A.10}$$

$$kg: 0 = 1 \cdot a_{21} + 0 \cdot a_{22} + 0 \cdot a_{23}, \tag{A.11}$$

$$m: 1 = -1 \cdot a_{21} + 2 \cdot a_{22} + 1 \cdot a_{23}, \tag{A.12}$$

$$s: -1 = -2 \cdot a_{21} - 1 \cdot a_{22} + 0 \cdot a_{23}. \tag{A.13}$$

which gives:

$a_{21} = 0$, $a_{22} = 1$, $a_{23} = -1$,

so the Π_2 equation obtains its final form as:

$$w = \Pi_2 p_o^0 v'^1 d^{-1} \Rightarrow \Pi_1 = \frac{w}{\frac{\eta}{\rho} \cdot \frac{1}{d}} = \frac{w\rho \cdot d}{\eta} = \mathrm{Re}_{TPF}. \tag{A.14}$$

v_p equation:

$$v_p = f\left(\Pi_1 \cdot \Pi_2\right) p_o^{b_1} \cdot v'^{b_2} \cdot d^{b_3}, \tag{A.15}$$

and the corresponding set of dimensional equations:

$$\left[kg^0 m^1 s^{-1}\right] = \left[kg^1 m^{-1} s^{-2}\right]^{b_1} \cdot \left[kg^0 m^2 s^{-1}\right]^{b_2} \cdot \left[kg^0 m^1 s^0\right]^{b_3}, \tag{A.16}$$

$$kg: 0 = 1 \cdot b_1 + 0 \cdot b_2 + 0 \cdot b_3, \tag{A.17}$$

$$m: 1 = -1 \cdot b_1 + 2 \cdot b_2 + 1 \cdot b_3, \tag{A.18}$$

$$s: -1 = -2 \cdot b_1 - 1 \cdot b_2 + 0 \cdot b_3 . \quad \text{(A.19)}$$

which gives:

$b_1 = 0$, $b_2 = 1$, $b_3 = -1$,

so the v_p obtains its form as:

$$v_p = f\left(\Pi_1 \cdot \Pi_2\right) p_o^0 \cdot \nu'^1 \cdot d^{-1}. \quad \text{(A.20)}$$

v_p can be further transformed into a dimensionless form:

$$\frac{v_p}{w} = C \cdot \Pi_1^B \cdot \Pi_2^C \cdot \Phi^D \quad \text{(A.21)}$$

$$\frac{v_p}{w} = C \cdot \left(\frac{w\rho \cdot d}{\eta}\right)^B \cdot \left(\frac{\Delta p}{p_o}\right)^C \cdot \Phi^D \quad \text{(A.22)}$$

The final result of the dimensional analysis is as follows:

$$v_p^+ = C \cdot \mathrm{Re}_{TPF}^B \cdot \left(\Delta p^+\right)^C \cdot \Phi^D . \quad \text{(A.23)}$$

The coefficients presented in this model were obtained using a non-linear regression method available in the Statistica software (Quasi-Newton and Symplex schemes).

The velocity of the temperature instabilities v_T depends on the following parameters:

$$v_T = f(\Delta T, T_o, \nu', d, w, \Phi). \quad \text{(A.24)}$$

Table A.2 contains the dimensional analysis of the parameters that influence the velocity of the temperature instability v_T.

Table A2. Dimensional analysis of parameters that influence the velocity of the temperature instability v_T.

Parameter	SI units			Role
	[K]	[m]	[s]	
v_T	0	1	-1	Target function
ΔT	1	0	0	Term of Π_1 eq.
T_o	1	0	0	Independent parameter
ν'	0	2	-1	Independent parameter
D	0	1	0	Independent parameter
w	0	1	-1	Term of Π_2 eq.
Φ	0	0	0	Dimensionless

The first step is to confirm that the selected independent parameters are independent. To do so, the determinant of the T_o, ν', d dimensions has to be a number other than zero:

$$\det\begin{bmatrix} 1 & 0 & 0 \\ 0 & 2 & -1 \\ 0 & 1 & 0 \end{bmatrix} = -1 \tag{A.25}$$

The next step is to derive formulas for the Π_1 and Π_2 dimensionless numbers.

Π_1 equation:

$$\Delta T = \Pi_1 T_o^{a_{11}} \nu'^{a_{12}} d^{a_{13}}, \tag{A.26}$$

and the corresponding set of dimensional equations:

$$\left[K^1 m^0 s^0\right] = \left[K^1 m^0 s^0\right]^{a_{11}} \cdot \left[K^0 m^2 s^{-1}\right]^{a_{12}} \cdot \left[K^0 m^1 s^0\right]^{a_{13}} \tag{A.27}$$

$$K: 1 = 1 \cdot a_{11} + 0 \cdot a_{12} + 0 \cdot a_{13}, \tag{A.28}$$

$$m: 0 = 0 \cdot a_{11} + 2 \cdot a_{12} + 1 \cdot a_{13}, \tag{A.29}$$

$$s: 0 = 0 \cdot a_{11} - 1 \cdot a_{12} + 0 \cdot a_{13}. \tag{A.30}$$

which gives:

$a_{11} = 1$, $a_{12} = 0$, $a_{13} = 0$

so the Π_1 equation obtains its final form as:

$$\Delta T = \Pi_1 T_o^1 v'^0 d^0 \Rightarrow \Pi_1 = \frac{\Delta T}{T_0}, \tag{A.31}$$

Π_2 equation:

$$w = \Pi_1 T_o^{a_{21}} v'^{a_{22}} d^{a_{23}}, \tag{A.32}$$

and the corresponding set of dimensional equations:

$$\left[K^0 m^1 s^{-1}\right] = \left[K^1 m^0 s^0\right]^{a_{21}} \cdot \left[K^0 m^2 s^{-1}\right]^{a_{22}} \cdot \left[K^0 m^1 s^0\right]^{a_{23}} \tag{Z4.31}$$

$$K: 0 = 1 \cdot a_{21} + 0 \cdot a_{22} + 0 \cdot a_{23}, \tag{A.33}$$

$$m: 1 = 0 \cdot a_{21} + 2 \cdot a_{22} + 1 \cdot a_{23}, \tag{A.34}$$

$$s: -1 = 0 \cdot a_{21} - 1 \cdot a_{22} + 0 \cdot a_{23}, \tag{A.35}$$

which gives:

$a_{21} = 0$, $a_{22} = 1$, $a_{23} = -1$

so the Π_2 equation obtains its final form as:

$$w = \Pi_2 T_o^0 v'^1 d^{-1} \Rightarrow \Pi_1 = \frac{w}{\frac{\eta}{\rho} \cdot \frac{1}{d}} = \frac{w\rho \cdot d}{\eta} = \mathrm{Re}_{TPF}, \tag{A.36}$$

v_T equation:

$$v_T = f\left(\Pi_1 \cdot \Pi_2\right) T_o^{b1} \cdot v'^{b2} \cdot d^{b3} \tag{A.37}$$

and the corresponding set of dimensional equations:

$$\left[K^0 m^1 s^{-1}\right] = \left[K^1 m^0 s^0\right]^{b_1} \cdot \left[K^0 m^2 s^{-1}\right]^{b_2} \cdot \left[K^0 m^1 s^0\right]^{b_3}, \tag{A.38}$$

$$K: 0 = 1 \cdot b_1 + 0 \cdot b_2 + 0 \cdot b_3, \tag{A.39}$$

$$m: 1 = 0 \cdot b_1 + 2 \cdot b_2 + 1 \cdot b_3, \tag{A.40}$$

$$s: -1 = 0 \cdot b_1 - 1 \cdot b_2 + 0 \cdot b_3. \tag{A.41}$$

which gives:

$b_1 = 0$, $b_2 = 1$, $b_3 = -1$,

so v_T obtains its form as:

$$v_T = f(\Pi_1 \cdot \Pi_2) T_o^0 \cdot \nu'^1 \cdot d^{-1}, \tag{A.42}$$

v_T can be further transformed into a dimensionless form:

$$\frac{v_T}{w} = C \cdot \Pi_1^B \cdot \Pi_2^C \cdot \Phi^D, \tag{A.43}$$

$$\frac{v_T}{w} = C \cdot \left(\frac{w\rho \cdot d}{\eta} \right)^B \cdot \left(\frac{\Delta T}{T_0} \right)^C \cdot \Phi^D. \tag{A.44}$$

and v_T obtains its final form as:

$$v_T^+ = C \cdot \mathrm{Re}_{TPF}^B \cdot \left(\Delta T^+ \right)^C \cdot \Phi^D. \tag{A.45}$$

The coefficients in this model were obtained using a non-linear regression method available in Statistica software (Quasi-Newton and Symplex_schemes).

REFERENCES

[1] W. Kuczyński, A. Denis, A regressive model for dynamic instabilities during condensation of pro-ecological environmentally friendly refrigerant R1234yf, International Journal of Heat and Mass Transfer, Volume 131, March 2019, Pages 822-835

[2] D. Jung, Energy and environmental crisis: let's solve it naturally in refrigeration and air conditioning. American Society of Heating, Refrigerating and Air-Conditioning Engineers, September 2008.

[3] Z. Bonca, D. Butrymowicz, W. Targanski, T. Hajduk, Guide: new refrigerants and heat carriers. Thermal, chemical and operational properties, IPPU MASTA, Gdansk 2004 (in Polish).

[4] The Bitner Company Report on Refrigerants, Edition 17, 2013 (in Polish).

[5] W. Kuczynski, H. Charun, Modeling of a two-phase region length of the condensation of R134a and R404A refrigerants in pipe mini-channels with periodic hydrodynamic instabilities, *Heat Transfer Engineering* 35(9), pp. 850–862, 2014.

[6] W. Kuczynski, Phenomena that accompany the condensation of R404A refrigerant in multiports during hydrodynamic instabilities, *International Journal of Heat and Mass Transfer* 55, pp. 7718–7727, 2012.

[7] W. Kuczynski, H. Charun, T. Bohdal, Influence of hydrodynamic instability on the heat transfer coefficient during condensation of R134a and R404A refrigerants in pipe mini-channels, *International Journal of Heat and Mass Transfer* 55, pp. 1083–1094, 2012.

[8] W. Kuczynski, Pressure wave propagation during the condensation of the R404A refrigerant in mini-condenser under periodic hydrodynamic disturbances, *International Journal of Heat and Mass Transfer* 67, pp. 404–415, 2013.

[9] R. Teng, P. Cheng, T.S. Zhao, Instability of condensate film and capillary blocking in small-diameter-thermosyphon condensers, *International Journal of Heat and Mass Transfer* 42, pp. 3071–3083, 1999.

[10] T. Zhang, J. Wen, Y. Peles, J. Catano, R. Zhou, M.K. Jensen, Two-phase refrigeration flow instability analysis and active control in transient electronics cooling systems, *International Journal of Multiphase Flow* 37, pp. 84–97, 2011.

[11] W. Kuczyński, Experimental research on condensation of R134a and R404A refrigerants in mini-channels during impulsive instabilities. Part I, *International Journal of Heat and Mass Transfer* 128, pp. 728–738, 2019.

[12] W. Kuczyński, Experimental research on condensation of R134a and R404A refrigerants in mini-channels during impulsive instabilities. Part II, *International Journal of Heat and Mass Transfer* 128, pp. 773–782, 2019.

[13] T. Bohdal, Bubble boiling in flow of refrigerating media, *Journal of Mechanical and Energy Engineering* 1(41), pp. 57–64, 2017.

[14] T. Bohdal, M. Kruzel, M. Sikora, Analysis of heat transfer coefficient during refrigerant condensation in vertical pipe mini-channel, *Journal of Mechanical and Energy Engineering* 1(41), pp. 65–70, 2017.

[15] T. Bohdal, M. Kruzel, M. Sikora, An investigation of heat transfer coefficient during refrigerants condensation in vertical pipe microchannel, *Journal of Mechanical and Energy Engineering* 1(41), pp. 163–170, 2017.

[16] T. Bohdal, H. Charun, M. Sikora, Empirical study of heterogeneous refrigerant condensation in pipe mini-channels, *International Journal of Refrigeration* 59, pp. 210–223, 2015.

[17] J.A. Boure, A.A. Fritte, M.M. Giot, M.L. Reocreux, Highlights of two-phase critical flow: on the links between maximum flow rates, sonic velocities, propagation and transfer phenomena in single and two-phase flows, *International Journal of Multiphase Flow* 3, pp. 1–22, 1976.

[18] J.A. Boure, A.E. Bergles, L.S. Tong, Review of two-phase flow instability, *Nuclear Engineering and Design* 25, pp. 165–192, 1973.

[19] L.Y. Cheng, D.A. Drew, R.T. Lahey, An analysis of wave propagation in bubbly two-component, two-phase flow, *Journal of Heat Transfer* 107, pp. 402–408, 1985.

[20] S.G. Kandlikar, S. Garimella, D. Li, S. Colin, M.R. King, *Heat transfer and fluid flow in mini-channels and microchannels*, Elsevier, 2006.

[21] S.G. Kandlikar, Microchannels and mini-channels – history, terminology, classification and current research needs. First International Conference on Microchannels and Mini-channels, New York, NY, 2003.

[22] S.G. Kandlikar, W.K. Kuan, D.A. Willistein and J. Borrelli, Stabilization of flow boiling in microchannels using pressure drop elements and fabricated nucleation sites, *Journal of Heat Transfer* 128(4), pp. 389–396, 2006.

[23] A. Bergles, S.G. Kandlikar, On the nature of critical heat flux in microchannels, *Journal of Heat Transfer* 127(10), pp. 101–107, 2005.

[24] A.E. Bergles, J.G. Collier, J.M. Delhaye, G.F. Hewitt, F. Mayinger, *Two-phase flow and heat transfer in the power and process industries*, Hemisphere Publishing Corporation, Washington, DC, 1981.

[25] Y.Y. Hsu, On the size range of active nucleation cavities on a heating surface, *Journal of Heat Transfer* 84, pp. 207–216, 1962.

[26] T. Bohdal, H. Charun, M. Kruzel, M. Sikora, High pressure refrigerants condensation in vertical pipe minichannels, *International Journal of Heat and Mass Transfer* 134 (2019) pp. 1250–1260.

[27] A. Koşar, C.J. Kuo, Y. Peles, Suppression of boiling flow oscillations in parallel microchannels with inlet restrictors, *Journal Heat of Transfer* 128(3), pp. 251– 260, 2006.

[28] R.M. Stoddard, A.M. Blasick, S.M. Ghiaasiaan, S.I. Abdel-Khalik, S.M. Jeter, M.F. Dowling, Onset of flow instability and critical heat flux in thin horizontal annuli, *Experimental Thermal and Fluid Science* 26, pp. 1–14, 2006.

[29] R.K. Das, S. Pattanayak, Determination and analysis from annular to intermittent flow in vertical tubes, *Canadian Journal of Chemical Engineering* 74, pp. 49–57, 1996.

[30] R.K. Das, S. Pattanayak, Electrical impedance method for flow region identification in vertical upward gas-liquid two-phase flow, *Measurement Science and Technology* 4, pp. 1457–1463, 1993.

[31] G.F. Hewitt, N.S. Hall-Taylor, *Annular two-phase flow*, Pergamon Press, New York, NY, 1970.

[32] T. Nulboonrueng, J. Kaewon, S. Wongwises, Two-phase condensation heat transfer coefficients of HFC-134a at high mass flux in smooth and micro-fin tubes, *International Communications in Heat and Mass Transfer* 30(4), pp. 577–590, 2003.

[33] H. v. Helmholtz, Verhandlungen der Naturhistorisch-Medizinischen, *Vereins zu Heidelberg* Bd III(16), 1863.

[34] J.W.S. Rayleigh, *Theory of sound*, Volume II, Edition 2, pp. 319–326, Macmillan, London, 1896.

[35] H.Z. Chen, M. Groll, S. Rësler, Micro heat pipes: experimental investigation and theoretical modeling. Proceedings of the 8th International Heat Pipe Conference, Beijing, pp. 396–400, 1992.

[36] P.A. Gauglitz, C.J. Radke, An extended evolution equation for liquid film breakup in cylindrical capillaries, *Chemical Engineering Science* 43, pp. 1457–1465, 1988.

[37] M. Ishii, I. Kataoka, Interfacial transfer in annular dispersed flow. Argonne National Laboratory, Report CONP-820811-2, 1980.

[38] M. Ishii, Study on flow instabilities in two-phase mixture. Argonne National Laboratory, Report ANL-76-23, 1976.

[39] M. Ishii, *Thermo-fluid dynamic theory of two-phase flow*, Eyrulles, Paris, 1975.

[40] V.P. Carey, *Liquid-vapor phase-change phenomena*, Hemisphere, Washington, DC, 1992.

[41] R.C. Mercredy, J.M. Wigdortz, L.J. Hamilton, Prediction and measurement of acoustic wave propagation in two-phase media, *Transactions of the American Nuclear Society* 13, pp. 672–673, 1970.

[42] S. Middleman, *Modeling axisymmetric flows: dynamics of films, jets and drops*, Academic Press, New York, NY, 1995.

[43] L.L. Vasilýev, S.V. Konev, R. Razek, Investigation of capillary blocking of heat-pipe condensers, *Heat Transfer – Soviet Research* 20, pp. 692–701, 1988.

[44] M. Sikora, Flow structures during refrigerants condensation, *Journal of Mechanical and Energy Engineering* 1(41), pp. 101–106, 2017.

[45] R. Laskowski, M. Jaworski, Maximum entropy generation rate in a heat exchanger at constant inlet parameters, *Journal of Mechanical and Energy Engineering* 1(41), pp. 65–70, 2017.

[46] M. Grabowski, E. Błachnio, Experimental studies on the effect of the enhancement of the heating surface on the heat transfer coefficient for boiling in closed volume, *Journal of Mechanical and Energy Engineering* 2(42), pp. 121–130, 2018.

[47] R.E. Henry, M.A. Grolmes, H.K. Fauske, Pressure-pulse propagation in two-phase one- and two-component mixtures. ANL-7792, 1971.

[48] S. Levy, Prediction of two-phase annular flow with liquid entrainment, *International Journal of Heat and Mass Transfer* 9, pp. 171–188, 1966.

[49] G.B. Wallis, The onset of droplet entrainment in annular gas-liquid flow. General Electric Report, No. 62 GL127, 1962.

[50] G. Wang, P. Cheng, A.E. Bergles, Effects of inlet/outlet configurations on flow boiling instability in parallel microchannels. *International Journal of Heat and Mass Transfer* 51, pp. 2267–2281, 2008.

[51] R.C. Mercredy, J.M. Wigdortz, L.J. Hamilton, Prediction and measurement of acoustic wave propagation in two-phase media, *Transactions of the American Nuclear Society* 13, pp. 672–673, 1970.

[52] S. Middleman, Modeling axisymmetric flows: dynamics of films, jets and drops, Academic Press, New York, NY, 1995.

[53] C.S. Martin, M. Padmanabhan, Pressure pulse propagation in two-component slug flow, *Journal of Fluids Engineering* 101, pp. 44–52, 1979.

[54] V. Starov, S.R. Kosvintsev, V.D. Sobolev, M.G Velarde, S.W. Joo, S.H. Davis, S.G. Bankoff, Long wave instabilities of heated falling films; two-dimensional theory of uniform layers, *International Journal of Fluid Mechanics* 230, pp. 117–146, 1991.

[55] W. Kuczynski, H. Charun, Modeling of a two-phase region length of the condensation of R134a and R404A refrigerants in pipe mini-channels with periodic hydrodynamic instabilities, *Heat Transfer Engineering* 35(9), pp. 850–862, 2014.

[56] L. Kukiełka, *Basics of engineering research*, Technical University of Koszalin Publishing House, Koszalin, 2000 (in Polish).

[57] I. Roeske-Słomka, *Basics of statistics*, Technical University of Koszalin Publishing House, Koszalin, 1999 (in Polish).

[58] Sobczak M.: Statistics. Second edition, revised. Communications Publishing Houses, Warsaw, Poland, (1994).

Nomenclature

ID – Internal diameter of the channel, m

f – Frequency of instabilities, $f = \frac{1}{T}$

p_o – Average saturation pressure of the refrigerant, kg/m·s^2

Δp – Amplitude of the pressure oscillations due to instabilities, kg/m·s^2

T – Wave period, s

T_o – Average saturation temperature of the refrigerant, K

ΔT – Amplitude of the temperature oscillations due to instabilities, K

w – Average velocity of the two-phase mixture, m/s

v_p – Velocity of the pressure instability, m/s

v_T – Velocity of the temperature instability, m/s

Greek symbols

λ – Wavelength, m

η – Dynamic viscosity of the two-phase mixture, kg/m·s

υ – Kinematic viscosity of the two-phase mixture, m^2/s

ρ – Density, kg/m^3

Subscripts

o – Average value

p – Pressure

T – Temperature

$+$ – Dimensionless parameter